Direct Parameter-Extraction Method for HBT Small-Signal Model

Sami Bousnina, *Student Member, IEEE*, Pierre Mandeville, *Member, IEEE*, Ammar B. Kouki, *Member, IEEE*, Robert Surridge, and Fadhel M. Ghannouchi, *Senior Member, IEEE*

***Abstract*—An accurate and broad-band method for the direct extraction of heterojunction bipolar transistor (HBT) small-signal model parameters is presented in this paper. This method differs from previous ones by extracting the equivalent-circuit parameters without using special test structures or global numerical optimization techniques. The main advantage of this method is that a unique and physically meaningful set of intrinsic parameters is extracted from the measured S-parameters for the whole frequency range of operation. The extraction procedure uses a set of closed-form expressions derived without any approximation. An equivalent circuit for the HBT under a forward-bias condition is proposed for extraction of access resistances and parasitic inductances. An experimental validation on a GaInP/GaAs HBT device with a 2×25 μm emitter was carried out, and excellent results were obtained up to 30 GHz. The calculated data-fitting residual error for three different bias points over 1–30 GHz was less then 2%.**

***Index Terms*—Broad-band parameter-extraction method, closed-form expressions, heterojunction bipolar transistors.**

I. Introduction

FOR THE development of microwave circuits using heterojunction bipolar transistors (HBTs), it is essential to use an accurate HBT equivalent-circuit model for simulating circuit performances. The properties of this model should satisfy the following criteria: 1) the topology of the equivalent circuit model has to be selected by considering the device electrical response and 2) the model parameters-extraction procedure should be efficient and systematic.

Several papers have reported HBT small-signal equivalent-circuit parameter-extraction methods. Most of them are based on numerical optimization routines aiming the best fit of the model-calculated S-parameters to the measured ones. However, the resulting parameter values might be nonphysical and most of the time depend on the of initial-guess values. In order to ovoid this problem, several authors have proposed some analytical or semianalytical parameter extraction techniques. Costa *et al.* described in [1] a direct parameter-extraction technique, where special test structures were designed and measured for the calculation of the parasitic parameters. The frequency dependency of the equivalent-circuit model parameters was discussed in [2], allowing a direct extraction of certain parameters. The remaining parameters (R_{be}, C_{be}, R_e, and L_e) are extracted using numerical optimization. An alternative approach for small-signal modeling of HBTs was also proposed in [3], where certain assumptions and optimization steps were used. Another direct extraction procedure for HBTs was developed in [4], where the effect of pad capacitances was neglected and the measured S-parameter under open-collector bias conditions were utilized to determine the extrinsic parameters. Recently, an approach combining analytical and optimization routines for parameter-extraction purposes was reported in [5], in which dc and multibias RF measurements are used in conjunction with a conditioned impedance-block optimization approach. Finally, Li *et al.*have proposed in [6] a parameter-extraction approach that combines analytical and empirical-optimization procedures. In this approach, the derived circuit equations are simplified by neglecting some terms depending on the frequency range (low–middle–high frequencies) where the model parameters are extracted.

Most of these techniques were based on the use of device's frequency behavior, but some assumptions and approximations are made in order to derive the equivalent-circuit equations. This introduces an uncertainty in the obtained parameter values depending on the accuracy and validity of the assumptions. In practice, and due to the diversity of the process technology and device geometry, these assumptions and approximations need to be modified and adjusted for different processes and devices. In order to design both analog and digital applications, an accurate and systematic extraction technique is essential to precisely model the device performance from dc to millimeter-wave frequencies [7].

Based on [8], this paper presents the essence with details of the HBT small-signal model extraction technique. This paper is organized as follows. In Section II, the methodology of deriving closed-form equations describing the intrinsic part of the device equivalent circuit is presented. Section III then discusses the basic procedure for extracting the small-signal element parameters. Section IV gives the extraction results and discussion. Conclusions are presented in Section V.

II. Theoretical Analysis

The HBT small-signal equivalent circuit is shown in Fig. 1. This circuit is divided into two parts, i.e., the outer part contains the extrinsic elements, considered as bias-independent, and the inner part (in the dashed box) contains the intrinsic elements, which are supposed to be bias dependent.

In order to facilitate the extraction of the intrinsic parameters, we compact the intrinsic part of the device equivalent circuit

Manuscript received September 18, 2000.

S. Bousnina and F. M. Ghannouchi are with the Département de génie électrique et de génie informatique, École Polytechnique de Montréal, Montréal, QC, Canada H3V 1A2.

P. Mandeville and R. Surridge are with Nortel Networks, Nepean, ON, Canada K1Y 4H7.

A. B. Kouki is with École de technologie supériere, Montréal, QC, Canada H3C 1K3.

Publisher Item Identifier S 0018-9480(02)01163-8.

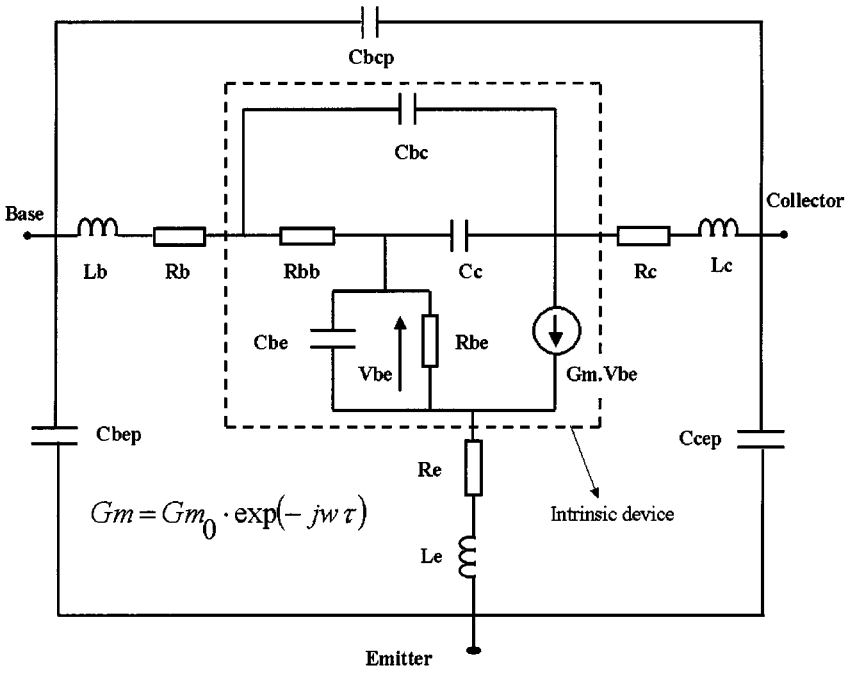

Fig. 1. Small-signal equivalent circuit of the GaInP/GaAs HBT.

shown in Fig. 2 using the well-known $T \leftrightarrow \Pi$ transformations shown in detail in Fig. 3. The final circuit is shown in Fig. 4.

Since the intrinsic device exhibits a Π topology, it is convenient to use the admittance (Y) parameters to characterize its electrical proprieties. These parameters are defined as follows:

$$Y_{11} = \frac{Z_1 + Z_4}{Z_1 \cdot Z_4} \tag{1}$$

$$Y_{12} = -\frac{1}{Z_4} \tag{2}$$

$$Y_{22} = \frac{Z_4 + Z_3}{Z_4 \cdot Z_3} + X \tag{3}$$

$$Y_{21} = X \cdot \frac{Z_3}{Z_1} - \frac{1}{Z_4}. \tag{4}$$

With $X = B \cdot G_{m_0} \cdot \exp(-jw\tau)$,

$$Z_A = R_{bb}$$
$$Z_B = \frac{1}{J\omega C_c}$$
$$Z_C = \frac{R_{be}}{1 + J\omega R_{be} C_{be}}$$
$$Z_{bc} = \frac{1}{J\omega C_{bc}}$$
$$Z_1 = \frac{D_2}{Z_B}$$
$$Z_2 = \frac{D_2}{Z_C}$$
$$Z_3 = \frac{D_2}{Z_A}$$
$$Z_4 = \frac{Z_2 Z_{bc}}{Z_2 + Z_{bc}}$$
$$D_2 = Z_A Z_B + Z_B Z_C + Z_A Z_C$$

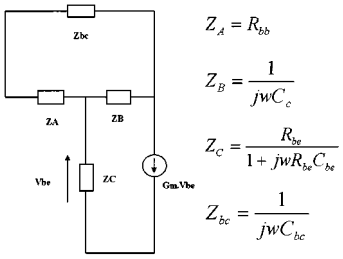

Fig. 2. Intrinsic part of the HBT small-signal model.

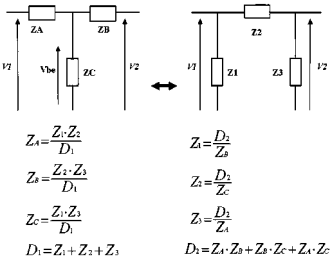

Fig. 3. Application of the $T \leftrightarrow \Pi$ transformations to the HBT device intrinsic equivalent circuit.

and

$$B = \frac{(Z_1)^2 Z_2 Z_3}{(Z_2)^2 Z_1 Z_3 + (Z_3)^2 Z_2 Z_1 + (Z_1)^2 Z_3 Z_2}.$$

III. Small-Signal Model Parameter Extraction

A. Extraction of Parasitic Elements

The first step in determining the equivalent-circuit elements is the accurate extraction of extrinsic element values. Some of the pad capacitances, pad inductances, and contact resistances are relatively small, but have significant influence on the extraction of the intrinsic elements. Thus, their values have to be

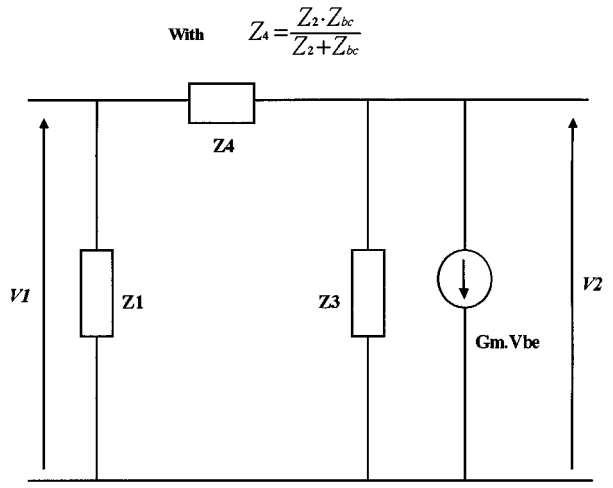

Fig. 4. Compacted equivalent circuit of the intrinsic HBT small-signal model.

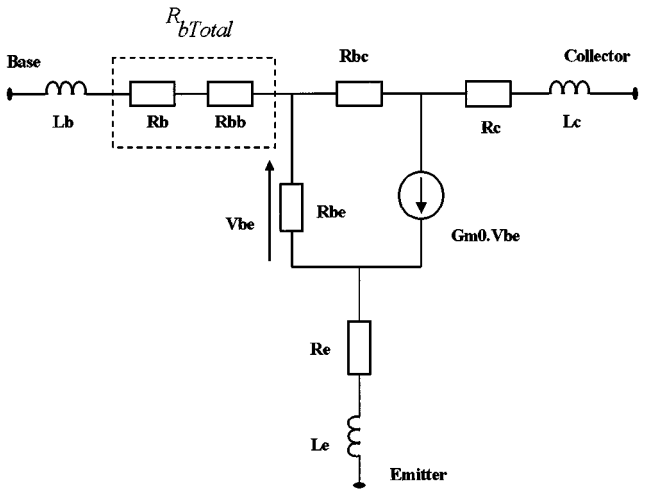

Fig. 5. Equivalent circuit of the HBT device at open-collector bias condition.

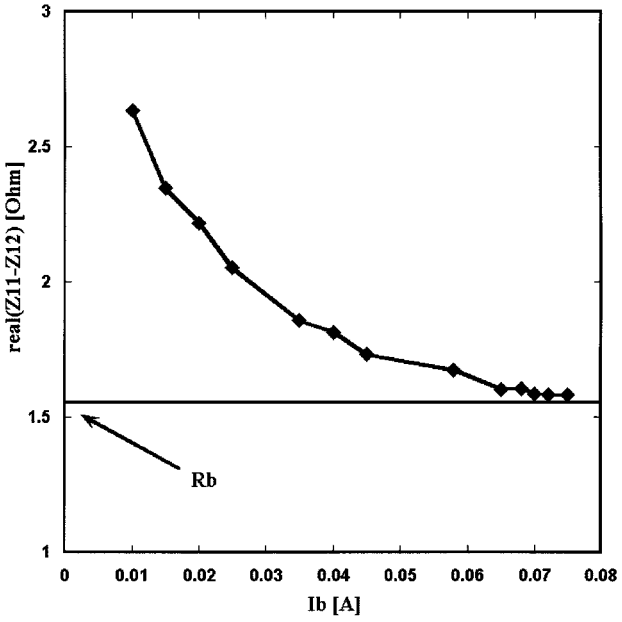

Fig. 6. Evolution of the total base resistance from $\mathrm{real}(Z_{11} - Z_{12})$ as a function of the current I_b, $\mathrm{freq} = 1.6$ GHz.

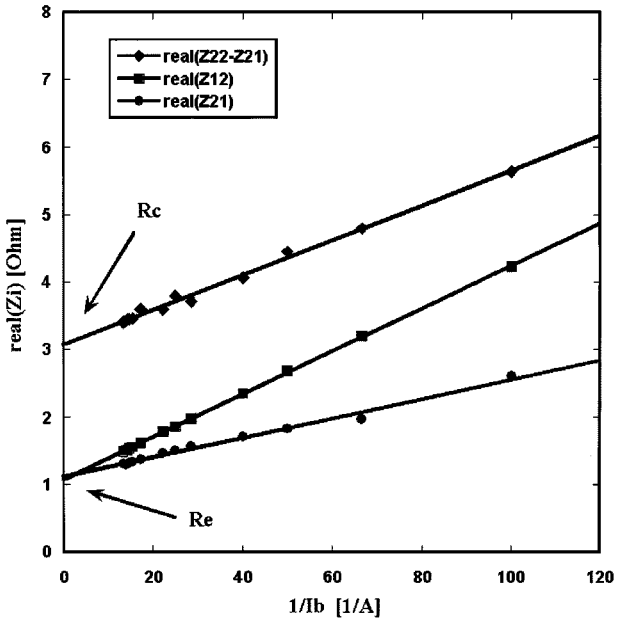

Fig. 7. Plot of $\mathrm{real}(Z_{12})$, $\mathrm{real}(Z_{21})$, and $\mathrm{real}(Z_{22} - Z_{21})$ versus $1/I_b$, $\mathrm{freq} = 1.6$ GHz.

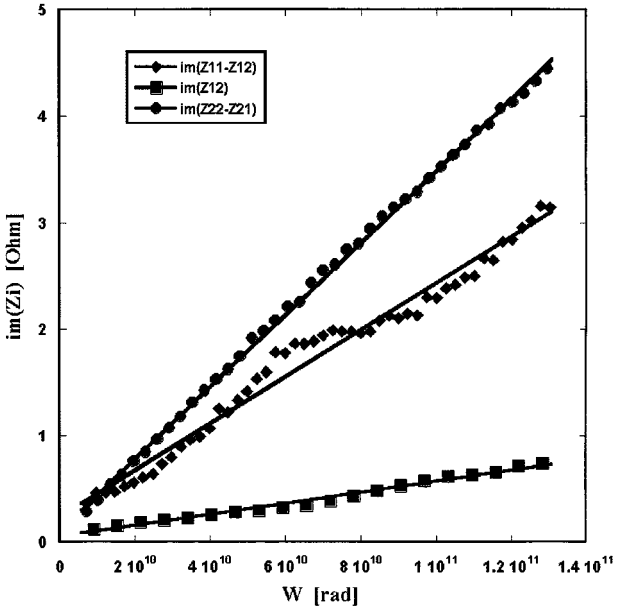

Fig. 8. Evolution of the imaginary part of the Z-parameters versus ω when the device is forward biased ($I_b = 60$ mA).

determined with great accuracy. As reported in [9], the extraction of parasitic elements is made by biasing the device first in forward operation (high current I_b) in order to extract the parasitic resistances (R_c, R_e, R_b) and inductances (L_c, L_e, L_b). The device is then biased in the cutoff operation mode a second time, thus permitting the extraction of the parasitic capacitances (C_{bep}, C_{bcp}, C_{cep}).

B. Extraction of Parasitic Inductances and Access Resistances

These parameters are determined from open-collector bias condition [4], where the base–collector and base–emitter junctions are in such forward condition that the collector current is

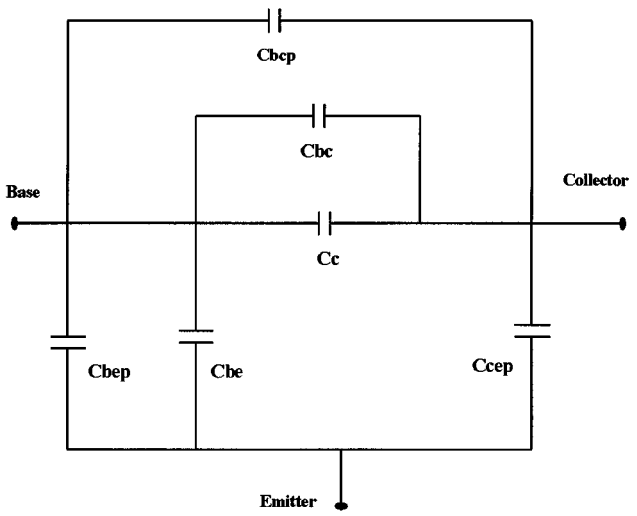

Fig. 9. Equivalent circuit of the reverse-biased HBT device.

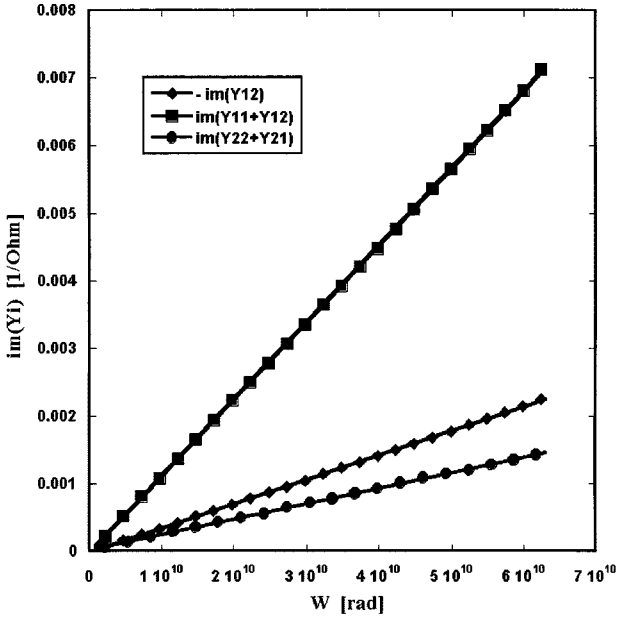

Fig. 10. Evolution of the imaginary part of the Y-parameters versus ω when the device is reverse biased ($V_{be} = -3$ V).

cancelled out. At high base current densities, the base–emitter and base–collector junctions capacitances have low impedances and low junction dynamic resistances short them. That is why the imaginary parts of Z-parameters of the equivalent circuit are dominated by the parasitic inductances of the device. In such an operation mode, the HBT equivalent circuit is shown in Fig. 5. This circuit is more valid than that used in [9] since it is not perfectly symmetric, more physical, and illustrates how to calculate with detail the different parameter values.

The Z-parameters of this circuit are defined by the following equations:

$$Z_{11} = R_{b\mathrm{Total}} + R_e + \frac{R_{be}}{1 + G_{m0} \cdot R_{be}} + jw \cdot (L_b + L_e) \tag{5}$$

$$Z_{12} = R_e + \frac{R_{be}}{1 + G_{m0} \cdot R_{be}} + jw \cdot L_e \tag{6}$$

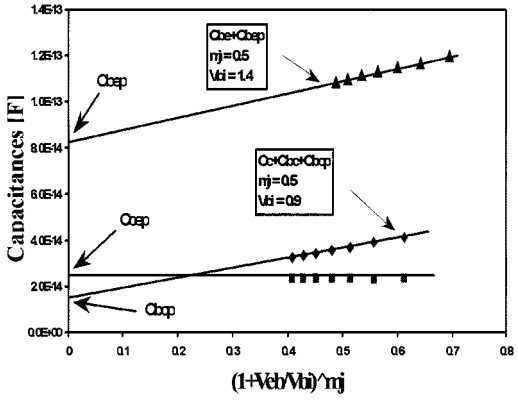

Fig. 11. Evolution of the measured capacitances ($C_c + C_{bc} + C_{bcp}$), ($C_{be} + C_{bep}$), and (C_{cep}) versus the expression $(1 - (V_{be}/V_{bi}))^{-m_j}$.

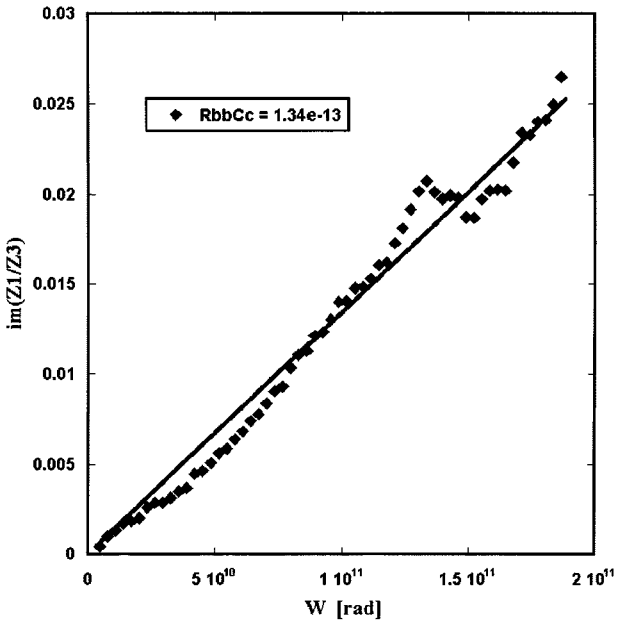

Fig. 12. Plot of $im(Z_1/Z_3)$ versus ω for the calculation of $R_{bb}C_c$ ($V_{ce} = 2$ V, $I_c = 10$ mA, $I_b = 50\ \mu$A).

$$Z_{21} = R_e + (1 - G_{m0} \cdot R_{bc}) \cdot \frac{R_{be}}{1 + G_{m0} \cdot R_{be}} + jw \cdot L_e \tag{7}$$

$$Z_{22} = R_c + R_e + \frac{R_{be}}{1 + G_{m0} \cdot R_{be}} \cdot \left(1 + \frac{R_{bc}}{R_{be}}\right) + jw \cdot (L_c + L_e) \tag{8}$$

where R_{be} and R_{bc} are dynamic resistances of the base–emitter and base–collector junctions, respectively, and their expressions are given as follows:

$$R_{be} = \frac{n_{be} KT}{q I_{be}} \tag{9}$$

$$R_{bc} = \frac{n_{bc} KT}{q I_{bc}}. \tag{10}$$

G_{m0} is the dc transconductance and $R_{b\mathrm{Total}}$ is the total base resistance, which depends on the injected forward base current I_b.

The extrinsic resistances are determined at low frequency from the real parts of the calculated Z-parameter as follows:

$$\mathrm{real}(Z_{11} - Z_{12}) = R_{b\mathrm{Total}} \tag{11}$$

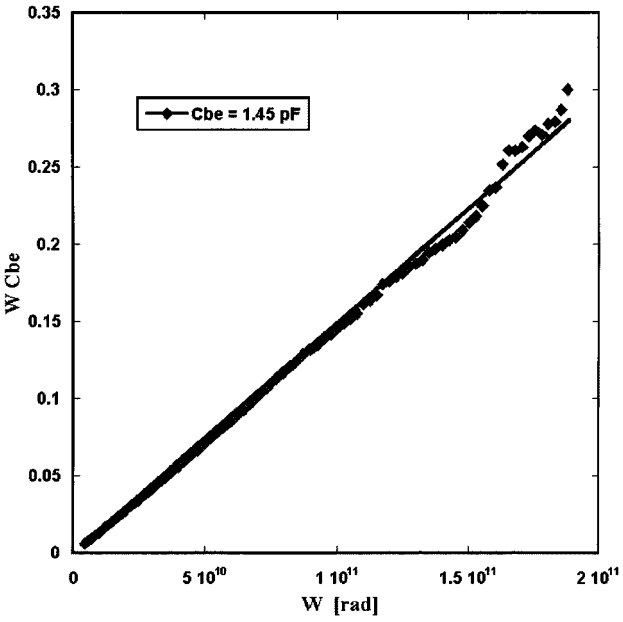

Fig. 13. Plot of ωC_{be} versus ω ($V_{ce} = 2$ V, $I_c = 10$ mA, $I_b = 50\ \mu$A).

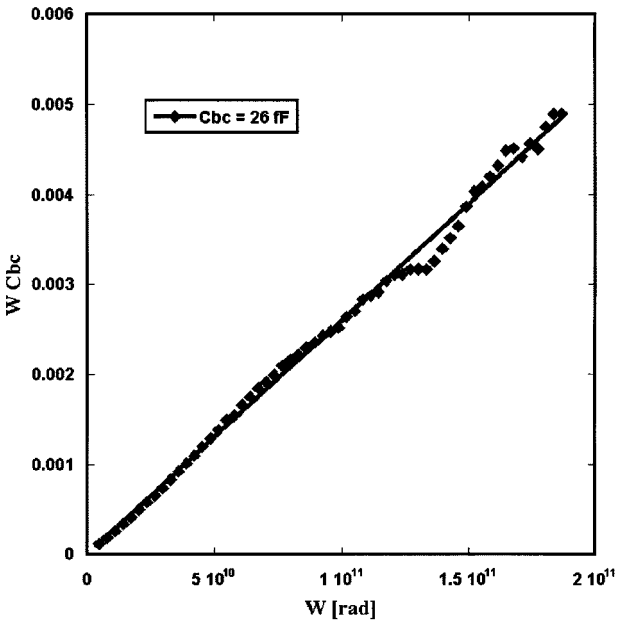

Fig. 15. Plot of ωC_{bc} versus ω ($V_{ce} = 2$ V, $I_c = 10$ mA, $I_b = 50\ \mu$A).

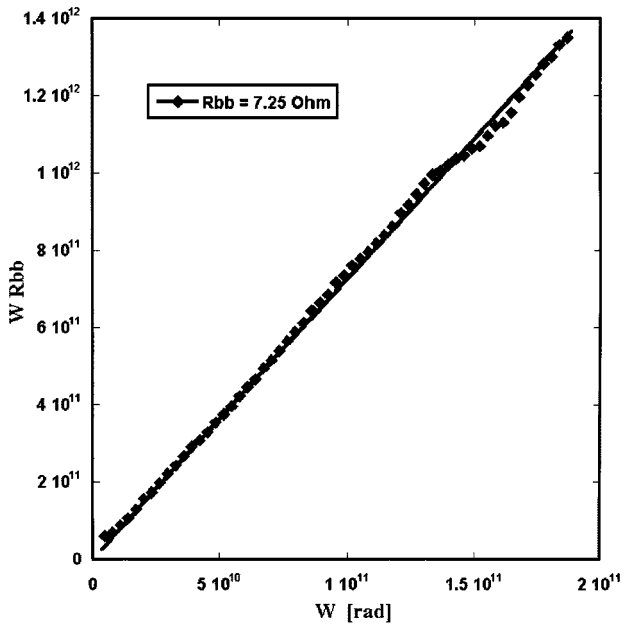

Fig. 14. Plot of ωR_{bb} versus ω ($V_{ce} = 2$ V, $I_c = 10$ mA, $I_b = 50\ \mu$A).

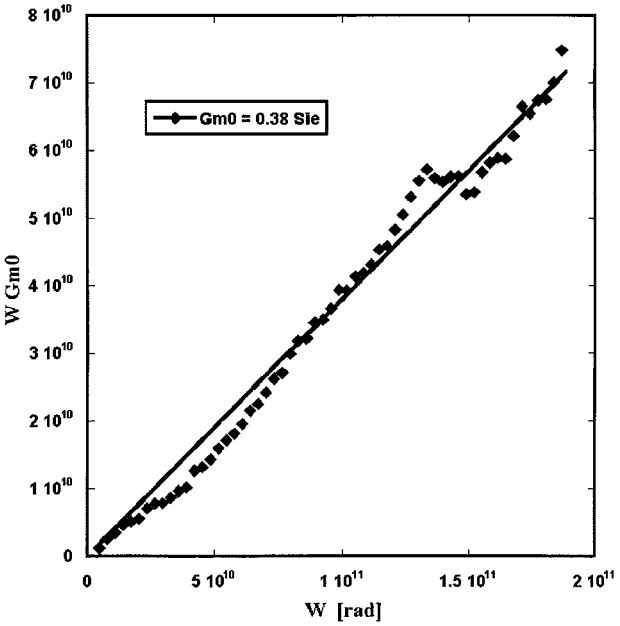

Fig. 16. Plot of ωG_{m0} versus ω ($V_{ce} = 2$ V, $I_c = 10$ mA, $I_b = 50\ \mu$A).

$$\text{real}(Z_{12}) = R_e + \frac{R_{be}}{1 + G_{m0} \cdot R_{be}} \tag{12}$$

$$\text{real}(Z_{22} - Z_{21}) = R_c + \frac{1}{1 + G_{m0} \cdot R_{be}} \cdot (R_{bc} + G_{m0} \cdot R_{bc} \cdot R_{be}). \tag{13}$$

At high base current densities I_b, the total base resistance $R_{b\text{Total}}$ tends asymptotically to the access base resistance R_b, as shown in Fig. 6. Also at these high current densities, R_{be} and R_{bc} became very small ($R_{be} \approx 0$, $R_{bc} \approx 0$) and the real part of Z_{12}, Z_{21}, and $Z_{22} - Z_{21}$ increase linearly as a function of $1/I_b$, as shown in Fig. 7. The extrapolated intercepts at the ordinate ($I_b \approx \infty$) of these lines give the value of R_e and R_c.

Fig. 7 shows also that the values of R_e extracted from the expressions of $\text{real}(Z_{12})$ and $\text{real}(Z_{21})$ are roughly the same, and the existent discrepancy between the evolution of these two expressions versus $1/I_b$ is explained by the fact the device at the considered bias condition is not perfectly symmetric as predicted by (6) and (7). For the parasitic inductances L_b, L_e, and L_c, using (5)–(8), one can easily get their values from the imaginary parts of $Z_{11} - Z_{12}$, Z_{12}, and $Z_{22} - Z_{21}$, respectively (Fig. 8).

C. Extraction of Parasitic Capacitances

The pad capacitances can be extracted or estimated from the HBT under cutoff operation [9]. Under such conditions, the

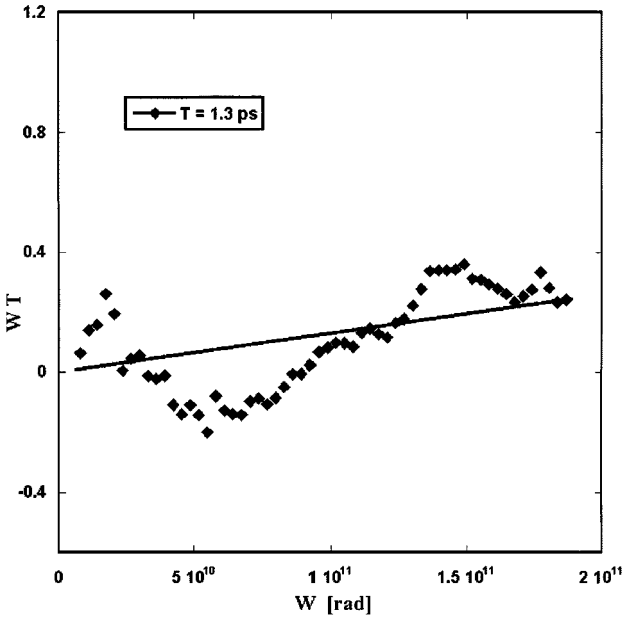

Fig. 17. Plot of $\omega\tau$ versus ω ($V_{ce} = 2$ V, $I_c = 10$ mA, $I_b = 50$ μA).

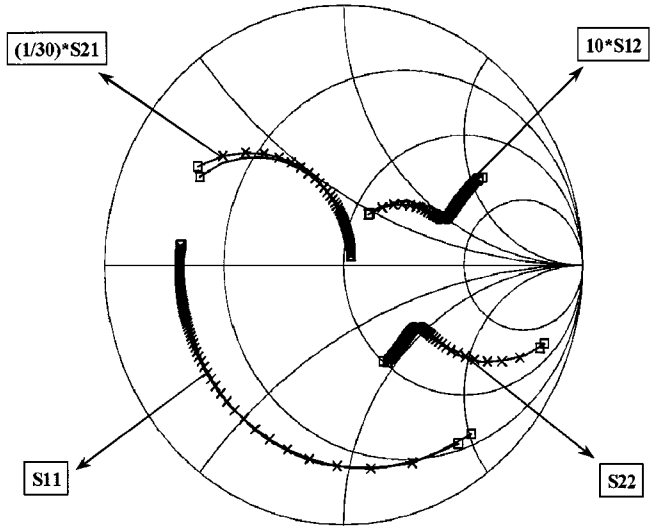

Fig. 18. Measured ($-$) and model-calculated ($-x-$) S-parameter of a 2×25 μm^2 HBT device (1–30 GHz, $V_{ce} = 2$ V, $I_c = 10$ mA, $I_b = 50$ μA).

HBT equivalent circuit of Fig. 1 is reduced to capacitance elements only, and can be represented by the circuit shown in Fig. 9.

From the Y-parameters of this circuit, we get

$$w \cdot (C_{bep} + C_{be}) = \text{imag}(Y_{11} + Y_{12}) \tag{14}$$

$$w \cdot (C_{bcp} + C_{bc} + C_c) = \text{imag}(Y_{22} + Y_{12}) \tag{15}$$

$$w \cdot (C_{cep}) = -\text{imag}(Y_{12}). \tag{16}$$

Fig. 10 shows the evolution of the Y-parameters of this circuit as a function of the frequency. In the above equations, the parameters C_{bep}, C_{bcp}, and C_{cep} are considered to be bias independent, while C_{be} and $C_{bc} + C_c$ (total base–collector junction capacitance) are bias-dependent elements. The output capacitance C_{cep} calculated from (16) keeps a constant value of 23.3 fF with varying the applied base voltage.

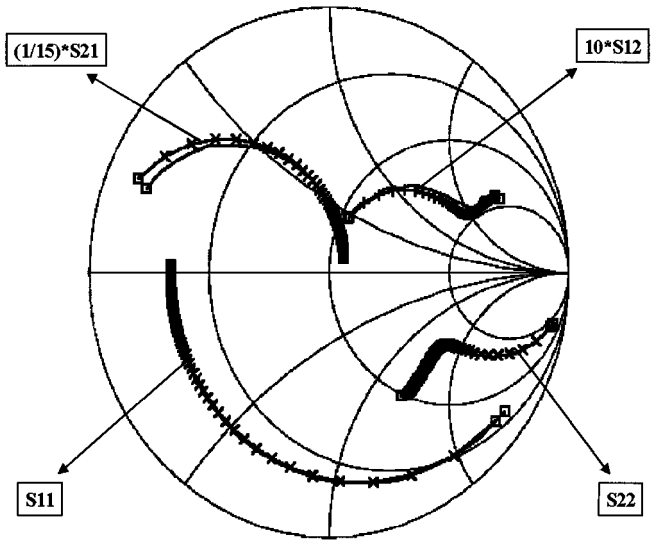

Fig. 19. Measured ($-$) and model-calculated ($-x-$) S-parameter of a 2×25 μm^2 HBT device (1–30 GHz, $V_{ce} = 3$ V, $I_c = 5$ mA, $I_b = 50$ μA).

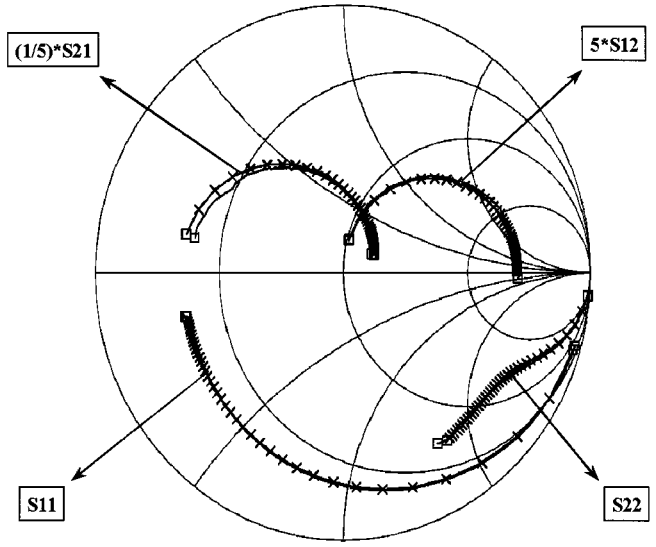

Fig. 20. Measured ($-$) and model-calculated ($-x-$) S-parameter of a 2×25 μm^2 HBT device (1–30 GHz, $V_{ce} = 3$ V, $I_c = 1$ mA, $I_b = 6$ μA).

Both the base–emitter and base–collector junction capacitances can be described by the following well-known expression:

$$C_j = \frac{C_{j0}}{\left(1 - \dfrac{V_{be}}{V_{bi}}\right)^{m_j}}. \tag{17}$$

The extraction of the parasitic capacitances C_{bep} and C_{bcp} are carried out by fitting $(C_{be} + C_{bep})$ and $(C_c + C_{bc} + C_{bcp})$ to the expression $(1 - (V_{be}/V_{bi})^{-m_j}$, and this can be done by varying iteratively the parameters values of m_j and V_{bi} until the resulting curve is a straight line. Thus, the extrapolated intercepts at the ordinate of these lines give the values of parasitic capacitance.

As shown in Fig. 11, the obtained values of C_{bep} and C_{bcp} are 82.9 and 14.5 fF, respectively. However, in the reality, and as mentioned in [5], it is difficult to distinguish between these

TABLE I
HBT SMALL-SIGNAL MODEL PARAMETER VALUES FOR THE EXTRACTED BIAS POINTS

	$V_{ce}=2$V, $I_c=10$ mA, $I_b=50$ μA	$V_{ce}=3$V, $I_c=5$ mA, $I_b=26.5$ μA	$V_{ce}=3$V, $I_c=1$ mA, $I_b=6$ μA
L_b [pH]	25	25	25
L_c [pH]	35	35	35
L_e [pH]	5.8	5.8	5.8
C_{cep} [fF]	23.3	23.3	23.3
R_b [Ω]	1.53	1.53	1.53
R_c [Ω]	3.2	3.2	3.2
R_e [Ω]	1.1	1.1	1.1
R_{bb} [Ω]	7.25	7.8	7.41
R_{be} [Ω]	565	1079	4766
C_c [fF]	18.5	17.05	20
C_{be} [fF]	26	23.4	22.1
C_{bc} [pF]	1.45	0.932	0.38
τ [ps]	1.3	2.1	3.2
G_{m0} [Sie]	0.38	0.178	0.035

TABLE II
RESIDUAL DATA-FITTING ERROR FOR THE EXTRACTED BIAS POINTS

Bias point	$V_{ce}=2$V, $I_c=10$ mA, $I_b=50$ μA	$V_{ce}=3$V, $I_c=5$ mA, $I_b=26.5$ μA	$V_{ce}=3$V, $I_c=1$ mA, $I_b=6$ μA
Residual error	1.7%	1.8%	1.8%

parasitic capacitances and their corresponding junction capacitances. That is why, in this extraction procedure, their values were fixed to be zero, and if their presence exists, it will be supposed to be absorbed by the junction capacitances.

D. Extraction of Intrinsic Elements

The calculated extrinsic parameters are then used to deembed the measured S-parameter of the device and deduce the intrinsic Y-parameters defined by (1)–(4). We then calculate the parameters Z_i $(i=1,3,4)$ and X using the following equations:

$$Z_1=\frac{1}{Y_{11}+Y_{12}} \tag{18}$$

$$Z_4=-\frac{1}{Y_{12}} \tag{19}$$

$$Z_3=\frac{Y_{21}+Y_{11}}{(Y_{11}+Y_{12})\cdot(Y_{22}+Y_{12})} \tag{20}$$

$$X=Y_{22}-\frac{(Y_{11}+Y_{12})\cdot(Y_{22}+Y_{12})}{Y_{21}+Y_{11}}+Y_{12}. \tag{21}$$

At this stage, the intrinsic parameters can be determined analytically for each bias point as follows.

- $R_{be}=(n_{be}KT/qI_b)$, where n_{be} is the ideality factor of the base–emitter junction.
- $\omega R_{bb}C_c=im(Z_1/Z_3)$. The value of $R_{bb}C_c$ is then calculated from the slope of this expression when plotted versus the angular frequency ω, as shown in Fig. 12.
- $$\mathrm{im}(Z_1)=-\frac{R_{be}(R_{be}\omega C_{be}-\omega R_{bb}C_c)}{1+(\omega C_{be}R_{be})^2}.$$
  This relation represents a second-degree equation as a function of ωC_{be} and it has one meaningful solution as follows:
$$\omega C_{be}=\frac{-R_{be}^2-\sqrt{R_{be}^4-4(\mathrm{im}(Z_1)-\omega R_{bb}C_cR_{be})\cdot\mathrm{im}(Z_1)R_{be}^2}}{2\mathrm{im}(Z_1)R_{be}^2}.$$
  The other solution is usually nonphysical or negative. The value of C_{be} is then calculated from the slope of this expression when plotted versus ω, as shown in Fig. 13.
- From the real part of Z_1, we get
$$\omega R_{bb}=\frac{\omega\left(\mathrm{real}(Z_1)\cdot\left(1+(\omega C_{be}R_{be})^2\right)-R_{be}-R_{bb}C_cR_{be}^2C_{be}\omega^2\right)}{(1+C_{be}^2R_{be}^2\omega^2)}.$$
  The value of R_{bb} is calculated from the slope of this expression when plotted versus ω, as shown in Fig. 14.

Knowing the previously calculated values of R_{bb}, C_c, C_{be}, and R_{be}, one can calculate the parameters Z_2 and B, and then calculate the value of C_{bc}, τ, and G_{m0} from the slopes of their corresponding expressions

$$\omega\cdot C_{bc}=\mathrm{im}\left(\frac{1}{Z_4}-\frac{1}{Z_2}\right)$$

$$\omega\cdot\tau=tg^{-1}\left(\frac{-\mathrm{im}\left(\frac{X}{B}\right)}{\mathrm{real}\left(\frac{X}{B}\right)}\right)$$

$$\omega\cdot G_{m_0}=\omega\cdot\sqrt{\left(\mathrm{real}\left(\frac{X}{B}\right)\right)^2+\left(\mathrm{im}\left(\frac{X}{B}\right)\right)^2}.$$

Figs. 15–17 show the calculated value of C_{bc}, τ, and G_{m0}.

IV. RESULTS AND DISCUSSION

In order to validate and to assess the accuracy of the proposed extraction technique, we investigated several 2×25 μm^2 GaInP/GaAs common emitter HBT devices. The measurements were performed with a microwave probing system and a vector network analyzer (VNA) over the frequency range 1–30 GHz. Figs. 18–20 show a comparison between the measured and calculated S-parameters for the bias points ($V_{ce}=2$ V, $I_c=10$ mA, and $I_b=50$ μA), ($V_{ce}=3$ V, $I_c=5$ mA, and $I_b=50$ μA), and ($V_{ce}=3$ V, $I_c=1$ mA, and $I_b=6$ μA) corresponding, respectively, to the operation classes A, AB, and B. Table I gives the small-signal model parameter's values for the extracted bias points. An excellent agreement over the whole frequency range was obtained. Table II gives the values of the

residual error quantifying the accuracy of the proposed extraction method accordingly to the following defined error function:

$$\|\vec{\varepsilon}\| = \frac{1}{4N} \sum_{i,\,j=1}^{2} \sum_{k=1}^{N} \frac{\left|S_{ij}^{m}(f_k) - S_{ij}^{c}(f_k)\right|}{\max_k \left(\left|S_{ij}^{m}(f_k)\right|\right)}$$

where N is the number of considered frequency points, $S_{ij}^{m}(f_k)$ is the measured S-parameter at the frequency f_k, and $S_{ij}^{c}(f_k)$ is the calculated corresponding S-parameter coefficient derived from extracted values of the model parameters.

V. Conclusions

A new analytical and accurate method for extracting the HBT small-signal model parameters has been presented. The extraction procedure allows for direct and fast calculation of a unique physically meaningful set of intrinsic parameters for the whole frequency range of operation. The presented extraction procedure can be easily implemented for automatic device characterization and process monitoring. The excellent agreement between the measured and the model-calculated S-parameter of a 2×25 μm emitter HBT device has proven the accuracy of the proposed extraction method.

Acknowledgment

The authors would like to thank Dr. A. Birafane, École Polytechnique de Montréal, Montréal, QC, Canada, for his helpful technical discussions regarding this paper.

References

[1] D. Costa, W. Liu, and J. S. Harris, Jr., "Direct extraction of the AlGaAs/GaAs heterojunction bipolar transistor small-signal equivalent circuit," *IEEE Trans. Electron Devices*, vol. 38, pp. 2018–2024, Sept. 1991.

[2] D. R. Pehlke and D. Pavlidis, "Evaluation of the factors determining HBT high-frequency performance by direct analysis of S-parameter data," *IEEE Trans. Microwave Theory Tech.*, vol. 40, pp. 2367–2373, Dec. 1992.

[3] U. Schaper and B. Holzapfl, "Analytic parameter extraction of the HBT equivalent circuit with T-like topology from measured S-parameter," *IEEE Trans. Microwave Theory Tech.*, vol. 40, pp. 493–498, Mar. 1995.

[4] C.-J. Wei and J. C. M. Huang, "Direct extraction of equivalent circuit parameters for heterojunction bipolar transistors," *IEEE Trans. Microwave Theory Tech.*, vol. 43, pp. 2035–2039, Sept. 1995.

[5] A. Samelis and D. Pavlidis, "DC to high-frequency HBT-model parameter evaluation using impedance block conditioned optimization," *IEEE Trans. Microwave Theory Tech.*, vol. 45, pp. 886–897, June 1997.

[6] B. Li, S. Prasad, L. Yang, and S. C. Wang, "A semianalytical parameter-extraction procedure for HBT equivalent circuit," *IEEE Trans. Microwave Theory Tech.*, vol. 46, pp. 1427–1435, Oct. 1998.

[7] R. Hajji and F. M. Ghannouchi, "Small-signal distributed model for GaAs HBT's and S-parameter prediction at millimeter-wave frequencies," *IEEE Trans. Electron Devices*, vol. 44, pp. 723–731, May 1997.

[8] S. Bousnina, P. Mandeville, A. B. Kouki, R. Surridge, and F. M. Ghannouchi, "A new analytical and broadband method for determining the HBT small-signal model parameters," in *IEEE MTT-S Int. Microwave Symp. Dig.*, June 2000, pp. 1397–1400.

[9] Y. Gobert, P. J. Tasker, and K. H. Bachem, "A physical, yet simple, small-signal equivalent circuit for the heterojunction bipolar transistor," *IEEE Trans. Microwave Theory Tech.*, vol. 45, pp. 149–153, Jan. 1997.

Sami Bousnina (S'01) was born in Elhamma, Tunisia. He received the Electrical Engineering degree and D.E.A. degree from the Ecole Nationale des Ingénieurs de Tunis, Tunis, Tunisia, and is currently working toward the Ph.D. degree at the Ecole Polytechnique de Montréal, Montréal, QC, Canada.

His main interests include characterization and modeling of microwave semiconductor active devices (HBTs and FETs) and design of high-efficiency power amplifiers. From May to November 1999, he was with Nortel Networks, Ottawa, ON, Canada, where he was an Intern involved with the HBT devices characterization and small-signal modeling.

Mr. Bousnina was a student finalist in the Student Paper Competition of the 2000 IEEE Microwave Theory and Techniques Society (IEEE MTT-S). He was the recipient of the National Scholarship presented by the Tunisian Government (1998–2001).

Pierre Mandeville (S'90–M'92) received the Ph.D. degree in electrical engineering from Cornell University, Ithaca, NY, in 1993.

In 1985, he joined Nortel Networks (then Bell Northern Research), Nepean, ON, Canada, where he was involved in molecular beam epitaxy and later chemical beam epitaxy of optoelectronic and high-speed electronic structures. In 1996, he joined the high-speed circuit design team and currently manages the Fiber Circuit Development Group.

Ammar B. Kouki (S'89–M'90), photograph and biography not available at time of publication.

Robert Surridge, photograph and biography not available at time of publication.

Fadhel M. Ghannouchi (S'84–M'88–SM'93) received the B.Eng. degree in engineering physics and the M.S. and Ph.D. degrees in electrical engineering from the Ecole Polytechnique de Montreál, Montreál, QC, Canada, in 1983, 1984, and 1987, respectively.

He is currently a Professor with the Département de génie électrique et de génie informatique, Ecole Polytechnique de Montreál, where, since 1984, he has taught electromagnetics and microwave theory and techniques. He has provided consulting services to a number of microwave companies. He is also the founder of AmpliX Inc., Montréal, QC, Canada, a company that offer linearization products and services to wireless and satcom equipment manufacturers. His research interests are in the areas of microwave/millimeter-wave instrumentation and measurements, nonlinear modeling of microwave active devices, and design of power and spectrum-efficient microwave amplification systems.

Dr. Ghannouchi is a Registered Professional Engineer in the province of Quebec, Canada. He is on the editorial board of the IEEE TRANSACTIONS ON MICROWAVE THEORY AND TECHNIQUES and has served on the Technical Committees of several international conferences and symposiums.